Applied Catalysis A: General 512 (2016) 52–62

Contents lists available at ScienceDirect

Applied Catalysis A: General

journal homepage: www.elsevier.com/locate/apcata

Influence of alumina precursor on the physico-chemical properties of V–Sb–P–W/Al_2O_3 catalyst studied for the ammoxidation of propane

Nagaraju Pasupulety[a,**], Hafedh Driss[b], Sharif F. Zaman[a,b], Yahia Abobakor Alhamed[a,b], Abdulrahim Ahmed Alzahrani[a,b], Muhammad A. Daous[a,b], Lachezar Petrov[a,*]

[a] SABIC Chair of Catalysis, King Abdulaziz University, P.O. Box 80204, Jeddah 21589, Saudi Arabia
[b] Chemical and Materials Engineering Department, Faculty of Engineering, King Abdulaziz University, P.O. Box 80204, Jeddah 21589, Saudi Arabia

ARTICLE INFO

Article history:
Received 22 September 2015
Received in revised form 6 December 2015
Accepted 10 December 2015
Available online 12 December 2015

Keywords:
Propane
V–Sb–P–W/Al_2O_3 catalyst
Ammoxidation
Propylene
Acrylonitrile

ABSTRACT

Influence of alumina precursor on active phase formation in $V_{1.0}$–$Sb_{3.5}$–$P_{0.5}$–$W_{1.0}$/50% Al_2O_3 catalyst was studied for the ammoxidation of propane in the temperature range of 490–530 °C at W/F = 2.8 g_{cat} s ml^{-1}. Three different alumina precursors such as, aluminum chloride (AlC), aluminum hydroxide (AlH) and aluminum nitrate (AlN) were employed in the study. The physico-chemical characterisitics of the synthesized catalysts were investigated by BET surface area-pore size method, XRD, FTIR, HAADF/EDS, NH_3 TPD-mass and XPS techniques. XRD result demonstrates $AlPO_4$ phase for all the three catalysts which was likely due to P interaction with alumina precursor. Formation of propylene and acrylonitrile (ACN) in this study was influenced by the nature of the active surface on Al_2O_3 synthesized from different precursors. Among the catalysts, AlC exhibited greater propane conversion (76%) and ACN selectivity (28%) at 530 °C. The higher activity of AlC was associated with (i) active surface enriched in V–Sb–W phase as established by XPS and HAADF/EDS results (ii) higher adsorption ability for NH_3 in the presence of residual chloride (coming from $AlCl_3$) followed by efficient nitrogen insertion in the intermediate molecule of propane to yield ACN. The surface with Sb–W–O related phase in AlN and AlH possibly contributes to the degradation of adsorbed propane/propylene and NH_3 to yield methane, ethane, ethylene, CO_x and NO_x. To our knowledge, this is the first report for the influence of alumina precursor on the active phase formation in V–Sb–P–W/Al_2O_3 catalyst studied for the propane ammoxidation.

1. Introduction

Acrylonitrile is industrially produced by the catalytic ammoxidation of propylene also known as SOHIO process [1]. In 2013, worldwide production of acrylonitrile reported as 6 million tons from propylene/propane [2]. Poly acrylonitrile is the major component of several industrial textile fibers synthesized from acrylonitrile monomers. It is also copolymerized with vinyl chloride to produce a wool like fibers which are used for blankets and sweaters. The future global demand-supply gap cannot be fulfilled by acrylonitrile-propylene based process alone due to the price increase of propylene feed-stock. Alternative feed stock based acrylonitrile synthesis can help to accomplish the upcoming demands for acrylonitrile fiber. Propane is more abundant and less expensive feed-stock compared to propylene, which can be directly converted into acrylonitrile by catalytic ammoxidation process [3–6]. An efficient catalyst composition is necessary to achieve acrylonitrile in useful yields from propane. Principally, two types of catalyst compositions are reported in the literature on propane ammoxidation (i) Mo–V–Nb–Te–O (ii) V–Sb–W/Al_2O_3. In the present study, our focus is on complex V–Sb–W/Al_2O_3 catalyst for propane ammoxidation. Further, the propane ammoxidation performance of V–Sb catalyst was improved by using excess amount of antimony oxide which, exists as Sb_2O_4 in the final catalyst [7].

Nilsson et al. [8,9] extensively studied V–Sb, V–Sb–Al and V–Sb–W/Al_2O_3 catalysts for propane ammoxidation reaction. According to the authors, propane adsorption followed by dehydrogenation to propylene and subsequent nitrogen insertion step to form acrylonitrile takes place on V-sites. Addition of Al and Sb primarily isolate V-sites to a suitable degree to avoid degradation of propane, propylene and ammonia. And incorporation of W tunes the V-sites in a direction that helps to improve the acrylonitrile formation. These authors [8] further reported rutile type of Sb(V,W)O_4 active phase for $V_{1.0}$–$Sb_{5.0}$–$W_{1.0}$/50%Al_2O_3 catalyst in propane ammoxidation. Recently, Mamedov studied the propane ammoxidation on W doped V–Sb/Al catalyst. According

* Corresponding author. Fax: +966 26952257.
** Corresponding author.
E-mail addresses: pasupulety@gmail.com (N. Pasupulety), lpetrov@kau.edu.sa, lachezarptrv@yahoo.com, petrov@ic.bas.bg (L. Petrov).

http://dx.doi.org/10.1016/j.apcata.2015.12.014
0926-860X/

to the author the improved ACN selectivity was due to the higher adsorption ability for NH_3 on W–V–Sb/Al surface compared to V–Sb/Al [10]. Centi et al. [11] have studied the propane ammoxidation on $VO_2P_2O_7$, V–Ti mixed oxide, V–Sb and Fe–Sb catalysts. They found high activity and ACN selectivity on vanadium phosphate and vanadium antimonite catalysts. Mikolajska et al. [12] have studied the vanadium phosphorus mixed oxides supported on Al_2O_3 for propane ammoxidation. The authors attributed the high activity of VPO to V^{+5} site stability and tuned acid-base properties on Al_2O_3 support. Bilde et al. [13] described the catalytic behavior of thermally induced Sb_2O_3 spread on V/Al catalyst in the propane ammoxidation and the greater acrylonitrile selectivity was endorsed to V–Al–SbO_4 rutile phase. Therefore, all the above studied catalysts in the propane ammoxidation showed the significant role of Al as an element in the active phase and/or as a support. Accordingly, catalysts of different performance can be obtained depending on the type of alumina precursor used. Thus, it is essential to study the characteristics and performance of V–Sb–W/Al_2O_3 catalyst obtained through different alumina precursors for propane ammoxidation.

Vanadium and molybdenum sites can be isolated to a certain extent by incorporation of phosphorous (P) and P also improves the acidity moderately which intern minimizes the complete oxidation of propane using VPO and V–Mo–P–O [10–12,14] catalysts. Keeping this in mind, in the present work, the influence of phosphorous addition and Al_2O_3 prepared from different alumina precursor on V–Sb–W phase was examined with the catalyst composition of $V_{1.0}$–$Sb_{3.5}$–$P_{0.5}$–$W_{1.0}$/50% Al_2O_3. The preparation method and the V–P–Sb–W atomic composition was adopted from the US patent obtained by Brazdil and Guttmann [7]. The physico-chemical characteristics of these catalysts was analyzed by BET-pore size method, XRD, NH_3-TPD-mass, XPS and HAADF-EDS techniques and correlated to propane ammoxidation activity and acrylonitrile selectivity.

2. Experimental

2.1. Reagents

Ammonium metavanadate (NH_4VO_3, assay ≥ 98%), antimony oxide (Sb_2O_3, assay ≥ 99%), Aluminum hydroxide dried gel ($Al(OH)_3$), ammonium tungstate ($(NH_4)_2WO_4$, assay ≥ 99.99%), di ammonium hydrogen phosphate ($(NH_4)_2HPO_4$, assay ≥ 99%), Aluminum chloride ($AlCl_3{\cdot}6H_2O$, assay ≥ 99%), ammonia solution (NH_4OH, 30 wt.%) and Nitric acid (HNO_3 60%) were purchased from ACROS chemical suppliers and used without further purification. The preparation method and the V–P–Sb–W atomic composition was adopted from the US patent obtained by Brazdil and Guttmann [7].

2.2. Catalyst preparation A

V–Sb–P–W (1:3.5:0.5:1 atomic ratio) containing 50% Al_2O_3 produced from aluminum hydroxide dry gel precursor (this considered as a base catalyst).

Step-1: 3.81 g of ammonium metavanadate was dissolved in 90.0 cm^3 of hot (80 °C) deionized water and followed by the addition of 16.6 g of Sb_2O_3 to this solution. The resulting slurry was refluxed for 17 h under continuous stirring. The color of the mixture turned to gray-green.

Step-2: 47.88 g of aluminum hydroxide (dried gel) was added to 140.0 cm^3 of 10% acetic acid and stirred for 3 h to form a homogeneous suspension. The suspension was kept under continuous stirring for 3 h. No gelling was observed. The pH of the slurry recorded as 6.0.

Step-3: 9.23 g of ammonium tungstate was dissolved partially in 20 cm^3 of deionized water and to this 5 cm^3 of di ammonium hydrogen phosphate (2.15 g) solution was added.

The slurry obtained from step-1 was slowly added to step-3 solution under continuous stirring. Later, the step-2 suspension was added to this solution quickly under continuous stirring. The excess water was evaporated under continuous stirring on a preheated oil bath at 120 °C. The resultant solid was dried in a preheated oven at 120 °C overnight in static air.

2.3. Preparation B

V–Sb–P–W (1:3.5:0.5:1 atomic ratio) containing 50% Al_2O_3 produced from aluminum chloride precursor.

Aluminum chloride was used instead of aluminum hydroxide (dry gel) in step-2 and reaming procedure was identical to preparation A.

Step-2: 47.8 g of $AlCl_3{\cdot}6H_2O$ was dissolved in 2.5 m^3 of deionized water. In another beaker 77.0 cm^3 of 12N ammonia solution was diluted with deionized water to 500 cm^3 and quickly added to the $AlCl_3$ solution under continuous stirring. As formed white gelatinous precipitate (pH 8.0) was aged for overnight. The resultant precipitate was separated by means of filtration and washed thoroughly with deionized water to remove the Cl^- ions. Further, 47.0 cm^3 of 10% acetic acid solution was added to the gel and the remaining steps were identical to preparation A.

2.4. Preparation C

V–Sb–P–W (1:3.5:0.5:1 atomic ratio) containing 50% Al_2O_3 produced from aluminum nitrate (aluminum hydroxide dry gel + HNO_3) precursor.

Synthesized, aluminum nitrate was used instead of aluminum hydroxide (dry gel) in step-2 and reaming procedure was identical to preparation A.

One hundred and forty cubic centimeter of 60% HNO_3 was added to 48 g aluminum hydroxide (dried gel) and the resulting solution temperature was maintained at 80 °C under continues stirring until the color of the solution turns to clear yellow which, is indicative of aluminum nitrate formation. Here, the resultant solution was weakly acidic (pH 5.0) due to the presence of excess HNO_3. The remaining steps were identical to preparation A.

Further, the powder samples were pelletized and sieved to 0.5–2.0 mm size and calcined at 350 °C, 5 h followed by 610 °C for 3 h under static air conditions.

For example, V–Sb–P–W (1:3.5:0.5:1 atomic ratio) containing 50% Al_2O_3 catalyst produced from aluminum hydroxide (dry gel) precursor denoted as AlH, likewise, for aluminum chloride precursor as AlC and aluminum nitrate precursor as AlN.

2.5. Catalyst characterization

The BET surface area and pore size distribution of calcined samples used in the present study were determined by using Quantachrome Nova Station adsorption equipment at liquid nitrogen temperature after out gassing the samples at 200 °C under the flow of N_2 for 2 h.

The X-ray patterns of the samples used in the present study were obtained on a EQUINOX 1000 inel XRD instrument using Co Kα = 1.7902 Å with X-ray source generator settings at 40 kV and 30 mA and real time acquisition for $2\theta = 110°$. The FTIR analysis of calcined AlN, AlH and AlC samples were performed on a Bruker Vertex 70/70 v FTIR spectrometer using a KBr pellet method.

High angle angular dark field (HAADF)-scanning transmission microscopy (STEM) and energy dispersive X-ray (EDS) analysis with focused/parallel beam results of calcined samples were collected on

Table 1
BET surface area, pore volume and EDS data for AlH, AlN and AlC samples.

Catalyst	BET (m^2/g)	Pore volume (cc/g)	*EDS composition atomic%			
			V	Sb	W	Cl
AlN fresh	174.0	0.200	21.0	58.0	21.0	–
AlH fresh	181.0	0.228	21.0	57.0	22.0	–
AlC fresh	192.0	0.275	19.0	61.0	18.0	2.0
AlC used	–	–	20.0	61.5	18.0	0.5

* Focused beam analysis of selected grid slots after excluding alumina.

Tecnai 200 kV D1234 SuperTwin microscope with camera length of 97 cm.

Ammonia Temperature Programmed desorption (NH_3-TPD) experiments were conducted on ChemBET Pulsar Automatic Chemisorption Analyzer (Quantachrome Instrument). Mass analysis was performed using ThermoStar^{TM} GSD 320 quad core mass spectrometer (Pfeiffer, Germany). The typical mass fragments input as follows: $m/z = 16$ (NH_2), $m/z = 17$ (NH_3), $m/z = 18$ (H_2O), $m/z = 28$(N_2), $m/z = 30$ (NO) and $m/z = 44$(N_2O). In a typical experiment, catalyst sample of 100 mg was placed in a quartz cell and pretreated at 200 °C in He flow (10 $cm^3\,min^{-1}$) for 2 h. Subsequently, the temperature of the sample was brought to 50 °C and saturated with 5 vol.% NH_3-N_2 for 1 h. Eventually, the sample was flushed with He flow (10 $cm^3\,min^{-1}$) for 1 h. Desorption of probe gas was performed over the temperature range of 50–600 °C at a ramping rate of 10 °C min^{-1}.The desorption stream was analyzed simultaneously using a TCD and mass detector by means of an automated split valve.

XPS results of calcined samples in a tablet form was collected on SPECS GmbH high vaccum multi-technique surface analysis system equipped with Al-monochromatic X-ray source. The charge neutralization was done with low angle energy electron flood gun. The reported result was based on C1s reference at 285.0 eV.

2.6. Propane ammoxidation procedure

Propane ammoxidation was performed in a 12.7 mm quartz reactor with wall thickness 1.13 mm. 4.6 g of catalyst with particle size 0.5–2.0 mm was charged between the two layers of quartz wool in the middle of the reactor. The bed height was about 8 cm. Quartz thermo well with 6.35 mm was inserted axially through the catalyst bed from the bottom of the reactor to monitor the reactor temperature. Another thermocouple was inserted from the top of the reactor to monitor the inlet feed temperature. Catalytic tests were performed in the temperature range of 490–530 °C at the total feed flow rate of 100 SCCM with W/F = 2.8 $g_{cat}\,s\,ml^{-1}$ (STP). The feed composition with 19.11% oxygen, 12.74% ammonia and 6.37% propane balanced helium was studied under the reaction conditions. All the connections leading and leaving from the reactor was maintained at 250 °C to avoid the condensation of acrylonitrile polymer. Blank tests were also performed under similar reaction conditions.

The product stream was analyzed by HP 6890 GC equipped with FID and TCD detectors with single oven programming. Non hydrocarbons of 1 ml injection volume (O_2, N_2, N_2O, CO, CO_2, NH_3 and H_2O) were analyzed by TCD equipped with Molseive and Porapak N columns with 10 port GSV control column reversal technique. Hydrocarbons of 0.25 ml injection volume (methane, ethane, ethylene, propylene, propane, acetonitrile, acrylonitrile, acrolein and acrylic acid) were analyzed using FID equipped with Porapak QS. The GC detectors and columns were pre calibrated with certified standard gas mixtures obtained from Abdulla Hashim suppliers, Saudi Arabia. The reported results were within the sample standard devastation of ±1% mass. Small amount of HCN formation was reported on V–Sb/Al_2O_3 and V–Sb–W/Al_2O_3 catalyst [7,9,13] hence HCN was not analyzed in the present study. The total selectivity for acetonitrile, acrolein and acrylic acid was found in between 3 and 6% in the present study. The carbon balance falls in the range of 95–98%. The conversion, selectivity and yield was calculated based on these formulae:

$$\%\text{Conversion} = \left(\frac{\text{moles consumed}}{\text{moles in the feed}}\right) \times 100$$

$$\%SP_i = \left(\frac{\text{moles of product}}{\text{moles of propane consumed}}\right) \times (\text{CR}) \times 100$$

$$\%YP_i = \left(\frac{\text{moles of product}}{\text{moles of propane in the feed}}\right) \times (\text{CR}) \times 100$$

where CR is the ratio of the carbon atoms in the product to the number of carbon atoms in the propane.

3. Results and discussion

3.1. BET surface area and pore size distribution study

The nitrogen physisorption isotherms, pore size distribution histogram and BET surface area information of AlN, AlH and AlC with 50% Al loading was presented in Fig. 1 and Table 1. The result reveals the clear influence of alumina precursor on BET surface area, pore volume and pore size of the catalyst samples. Fig. 1 illustrates the pore size DFT area histogram with tri model pore distribution. All the three catalysts showed few number of micro and narrow sized mesopores in the pore width rage of 12–20 Å and 20–40 Å, respectively. The large size mesopores were distributed in the range of 40–100 Å on AlN and AlH with average pore width of 53 and 65 Å, respectively. On the other hand, wide spread distribution of large size mesopores (40–200 Å averaged at 80 Å pore width) observed on AlC. The maximum mesopore volume of 0.275 cc/g was obtained on AlC followed by AlH (0.228 cc/g) and AlN (0.200 cc/g). Fig. 1 inset displays the type-IV isotherm for all the three samples which is the characteristic feature of mesopore capillary condensation with mono-multi layer adsorption [16]. The shift in the hysteresis loop with respect to relative pressure under similar physisortion conditions indicates the mesopore size variation in the samples. The decreasing order of estimated BET surface area for these samples as follows: AlC (192.0 m^2/g) > AlH (181.0 m^2/g) > AlN (174.0 m^2/g). The result shows that Al_2O_3 produced from $AlCl_3$ generates greater BET surface area, large size mesopores with high volume. This might be associated with different degree of interaction between Al_2O_3 and the active species.

3.2. XRD study

Fig. 2 displays the X-ray pattern for fresh AlN, AlH and AlC samples. The fresh AlC catalyst was partially X-ray crystalline and the degree of crystallinity found to be higher in fresh AlN and AlH catalysts under similar XRD conditions (2 h of analysis, 30 mg of each catalyst). In all the three samples, X-ray patterns pronounced due to $AlPO_4$ [PDF 01-088-1680] and γ-Al_2O_3 [PDF 00-050-0741]

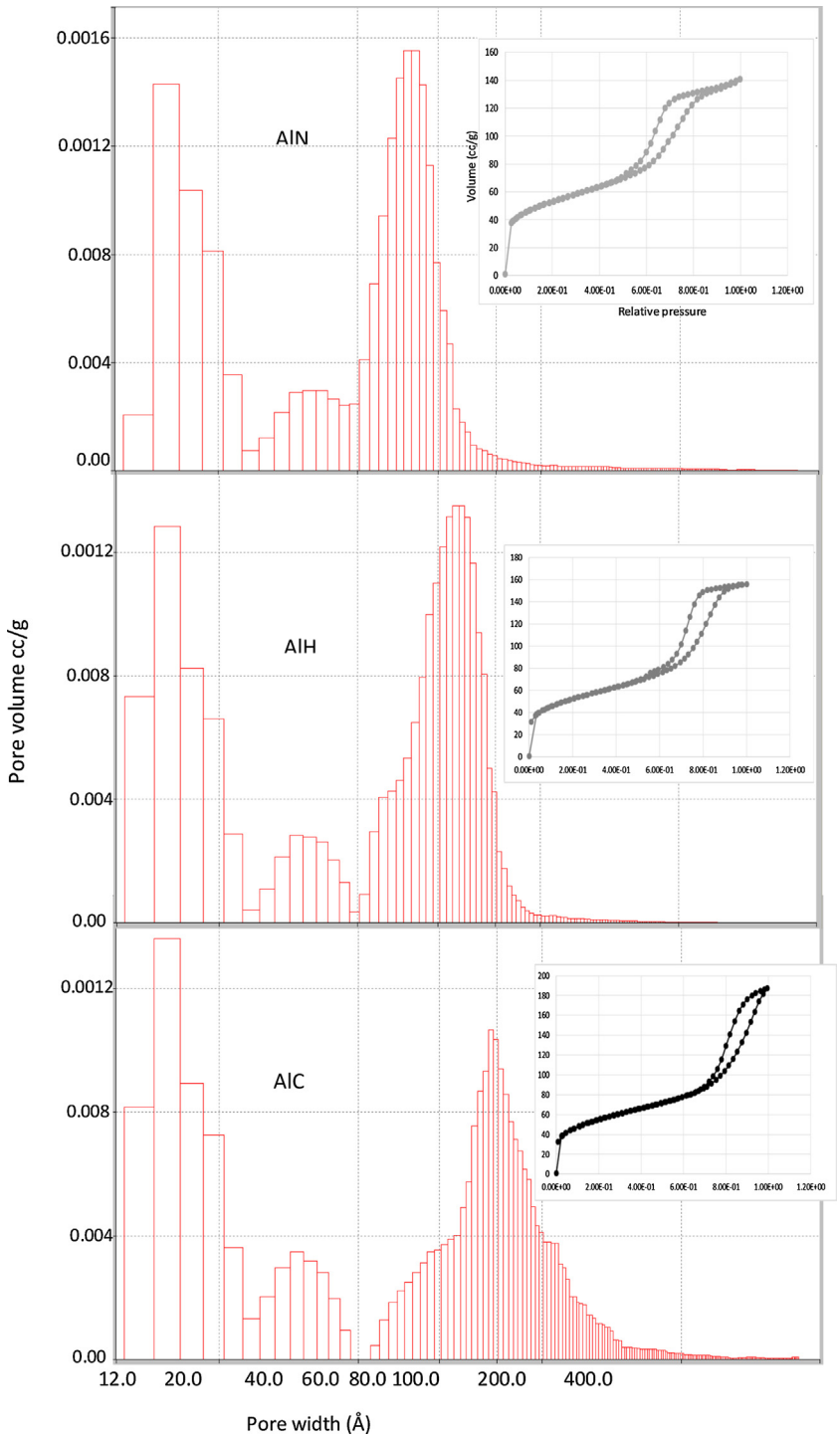

Fig. 1. Pore size DFT area histogram and inset shows adsorption isotherms for AlN, AlH and AlC.

phases. The addition of phosphorous to V–Sb–W/Al_2O_3 catalyst generated aluminum phosphate ($AlPO_4$) by the interaction of phosphorous with alumina precursor during the catalyst synthesis and/or thermal pretreatment. Further, the Al_2O_3 obtained from aluminum chloride precursor showed broad X-ray patterns compared to Al_2O_3 synthesized from aluminum hydroxide and aluminum nitrate. The broadening of X-ray pattern indicates the presence of dispersed/small sized Al_2O_3 crystallite. In all the three catalysts vanadium exists as -VO_2 [PDF 01-071-0289], antimony present in the form of Sb_2O_3 [PDF 01-075-1565]/Sb_2O_4 [PDF 01-071-0564] and W exists as WO_3 [01-088-0545] phase. Similar phases were reported by Guojuna et al. [15] for fresh V–Sb_3–W/Al_2O_3 catalyst. However, there were few differences observed in the X-ray pattern of the studied catalysts with respect to alumina precursor used. Aluminum nitrate primarily produces Sb_2O_4 and an unknown phase, whereas, aluminum hydroxide principally produces Sb_2O_3, Sb_2O_4 and an unknown phase in the final catalyst. On the other hand, aluminum chloride primarily produces Sb_2O_4 phase in the final catalyst. The variation in the intensities and FWHM for V, W and Sb phases in all the three catalyst indicates the difference in the crystallite size/dispersion of V–Sb–W related phase on their corresponding Al_2O_3. No X-ray patterns detected for V–P–O

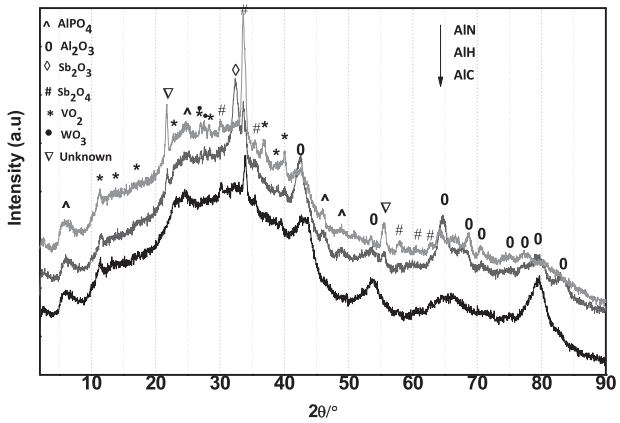

Fig. 2. XRD patterns for fresh AlN, AlH and AlC samples.

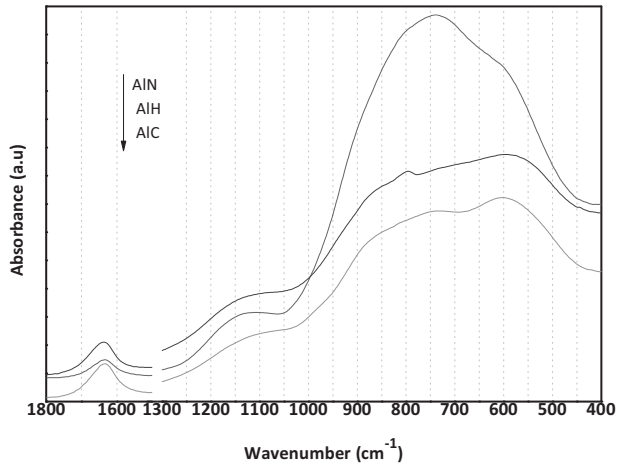

Fig. 3. FTIR spectra for AlN, AlH and AlC samples.

related phases. It is clear from the XRD results that the phase growth and direction was influenced by the alumina precursor in V–Sb–W/Al_2O_3 catalyst.

3.3. FTIR study

Fig. 3 illustrates the FTIR results of fresh AlN, AlH and AlC catalysts. A broad infrared band observed in the finger print region of 400–1050 cm^{-1} with shoulders at 600, 725, 800, 880, 1130 and 1625 cm^{-1} for all the three samples. The shoulder at 600 cm^{-1} was attributed to symmetric vibration of Sb_2O_3 [17] and/or related to AlO_4/AlO_6 vibrations [18]. The shoulder at 800 cm^{-1} associated with W—O—W bending vibrations [17]. The band at 1130 cm^{-1} ascribed to P—O stretching vibration for PO_4 group in $AlPO_4$ [19]. The shoulders appeared at 725 and 880 cm^{-1} were attributed to V—O vibrations in VO_2 and V_4O_9 species, respectively [20]. Further, the broad nature of finger print band cannot eliminate the presence of other V=O (923 and 1005 cm^{-1}) vibrations in these catalysts. The FTIR results are in agreement with XRD data.

3.4. HAADF/EDS study

Fig. 4 demonstrates the HAADF/EDS analysis of fresh AlN, AlH and AlC, catalysts. EDS analysis of these samples accomplished under focused beam unless otherwise stated. Fig. 4a and b displays 4 types of particle morphologies for AlN and AlH samples. They are nebulous, warm like, patch and near pyramidal type particles. EDS analysis of nebulous as well as warm like well-structured particles revealed as aluminum oxide. These are aggregated nano particles characterized by Al–O–Al linkages. EDS analysis of patches revealed the presence of V, Sb, W and oxygen components after excluding Al which comes from support Al_2O_3. Interestingly, the patches existed close to each other and chained to form a triangular shape on the surface of Al_2O_3. The approximate width of each patch in AlH found to be in the range of 60–80 nm with length 100–250 nm. However, for AlN the individual patch found to be much bigger compared to AlH and AlC with 100–120 nm width and 125–300 nm length. Further, EDS analysis of near pyramidal shaped particles revealed the presence of Sb, W and O components and the corresponding particle composition was comparable to -$Sb_{0.15}(WO_3)$ [21]. In addition, the unknown phase X-ray patterns (Fig. 2) for AlH and AlN at $2\theta = 23.0$ and 56.0° are also comparable with -$Sb_{0.15}(WO_3)$ X-ray patterns [21]. The size of these particles found to be in the range of 100–200 nm. On the other hand, only two different particle morphologies obtained on AlC catalyst (Fig 4c). The nebulous type mainly ascribed to aluminum oxide and patch type particles were associated with V, Sb, W and oxygen components (Fig. 4c, EDS graph). For AlC, the individual patch width and length exists in the range of 20–60 nm and 80–200 nm, respectively. The patch type morphology was also observed by Nilsson et al. [8] for rutile type Sb(V,W)O_4 phase in $V_{1.0}Sb_{5.0}W_{1.0}$/50% Al_2O_3 catalyst. However, those patches were irregular unlike the present study. Thus, we believe that the patches in this study with V, Sb, W and O components might be associated with a kind of rutile phase. The average EDS composition of five selected triangular patches for AlN, AlH and AlC samples are listed in Table 1. The parallel beam EDS analysis of selected slots revealed P along with Al, V, Sb, W and oxygen components for all the three samples. The result suggests that P is coming from the surrounding $AlPO_4$ (as evidenced by XRD) present in the final catalyst. Further, the chloride existence on AlC (Table 1) was likely due to the residue of $AlCl_3$. The HAADF/EDS result suggests the surface enrichment in V–Sb–W phase on Al_2O_3 synthesized from alumina chloride precursor. Whereas, V–Sb–W and Sb–W–O related phase existed on Al_2O_3 synthesized from aluminum nitrate and aluminum hydroxide precursor.

3.5. XPS study

Table 2 presents the surface compositions of V $2p_{3/2}$, Sb $3d_{3/2}$, P2p, W $4d_{5/2}$ and Al 2p for fresh AlN, AlH and fresh/spent AlC catalysts. After subtracting W 5s and V 3s binding energy (BE) from the Al 2p XPS signal, it showed BE at 74 ± 0.1 eV indicates the presence of Al^{+3} species. For, P 2p the BE recorded at 133 ± 0.1 eV attributed to P^{+5} species in all the three samples. After subtracting the Sb $3d_{5/2}$ and V $2p_{1/2}$ signal from O1s XPS signal, the shirley deconvolution generated a pair of signals at 530.5 and 532.8 eV. The earlier signal related to lattice oxygen (O^{-2}) and the later one ascribed to isolated (O^-) oxygen species. The O1s BE for $AlPO_4$ reported at 532.8 eV [22]. According to the Ref. [23], V $2p_{3/2}$ XPS signal for bulk V_2O_5 (V^{+5}) was narrow and appeared at 517.2 eV with 1.2 eV full width half maxima (FWHM). For bulk VO_2, V $2p_{3/2}$ BE and FWHM was reported as 516 and ≈2 eV, respectively. The broad nature of V $2p_{3/2}$ signal in VO_2 (V^{+4}) and V_2O_3 (V^{+3}, FWHM > 3 eV) was associated with multiplet configurations in the photoemission final states related to the core hole-3d electron interactions [23]. In the present study, the FWHM for V $2p_{3/2}$ measured greater than 3 eV in all the three catalysts. After shirley deconvolution of V $2p_{3/2}$ (V $2p_{1/2}$ to V $2p_{3/2}$ peak ratio 1:2) signal, it exhibits mainly V^{+5} and V^{+4} species on the surface of Al_2O_3. The V^{+4} recorded BE was in the range of 516.1–516.3 eV and for V^{+5} it was in the range of 517.2–517.4 eV for all the three catalysts. However, the V$2p_{1/2}$ signal showed FWHM of 2.0 eV and it was merged with O 1s/Sb$3d_{5/2}$ signal. Therefore, it was very complex to fit one more peak through shirley deconvolution to see the possibility of V^{+3} species on Al_2O_3 in all the three catalysts.

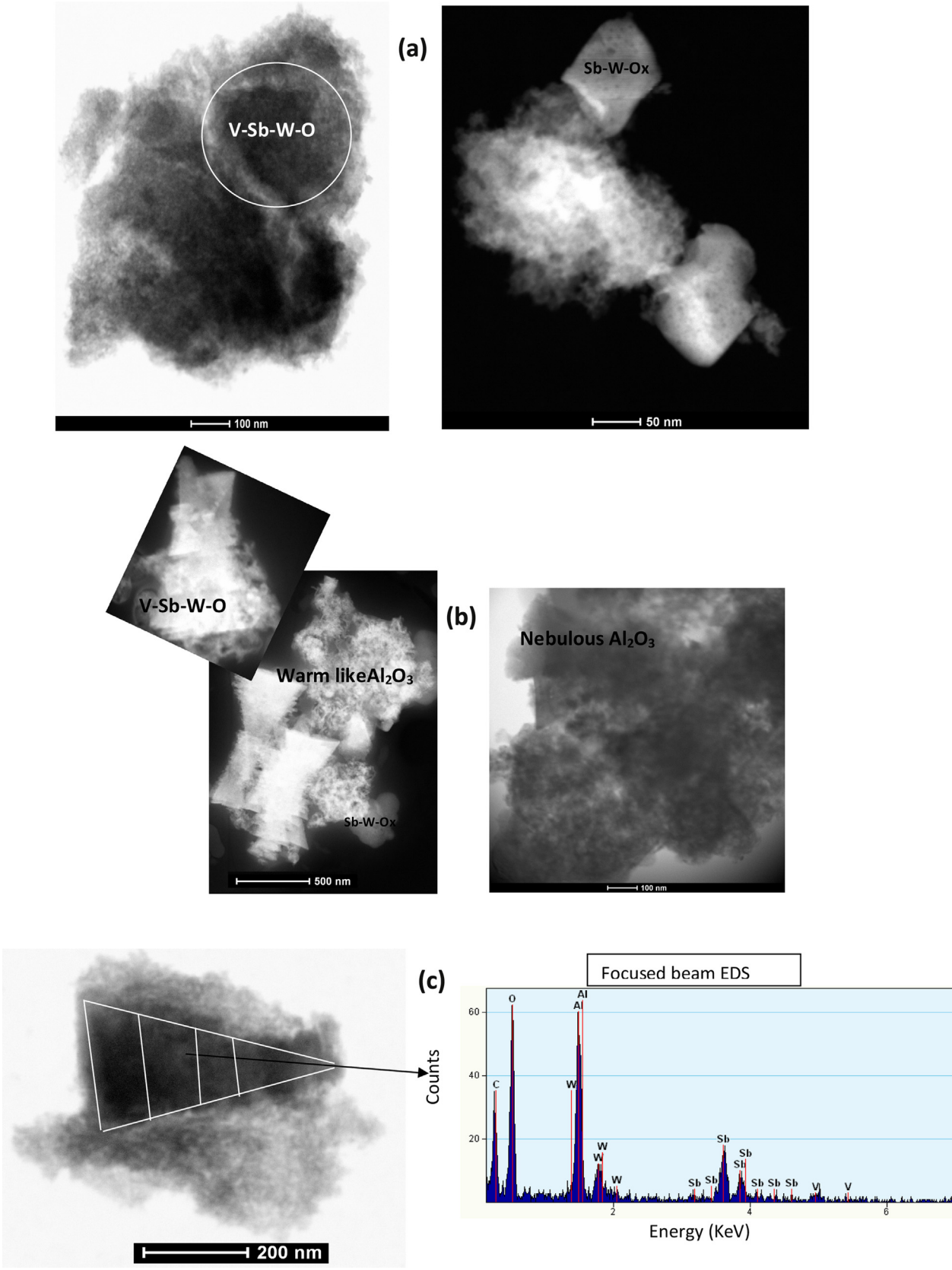

Fig. 4. HAADF/EDS images for (a) AlN (b) AlH and (c) AlC samples.

The shirley deconvolution of Sb $3d_{3/2}$ was based on the peak ratio of 2:3 between Sb $3d_{3/2}$ and Sb $3d_{5/2}$. All the three catalysts majorly showed Sb^{+4} species with small portion of Sb^{+5} species in the BE range of 540.3–540.4 eV and 540.5–540.9 eV, respectively. Nilsson et al. reported Sb $3d_{3/2}$ BE at 540.4 eV for Sb_2O_4 and at 540.8 eV for Sb_2O_5 [24]. WO_3 showed the W $4d_{5/2}$ BE at 247.7 eV and

Table 2
XPS data for AlH, AlN and AlC samples.

Catalyst	Surface composition atomic%									
	$V2p_{3/2}$		$Sb\ 3d_{3/2}$		$P^{+5}2p$	$W^{+4/+6}4d_{5/2}$	$Al^{+3}2p$	$Cl^{-}2p198$ eV	O 1s	
	V^{+5}	V^{+4}	Sb^{+5}	Sb^{+4}					O^{-2}	OH, O^{-}
AlN fresh	0.70	0.65	1.0	9.5	1.0	1.20	14.0	–	47.0	25.0
AlH fresh	0.60	0.80	1.4	11.1	1.2	1.23	15.6	–	43.0	25.0
AlC fresh	0.55	0.92	2.0	11.0	1.0	1.97	19.5	0.12	41.6	21.0
Used	0.41	1.2	2.9	10.6	1.2	3.0	22.0	0.10	39.6	19.0

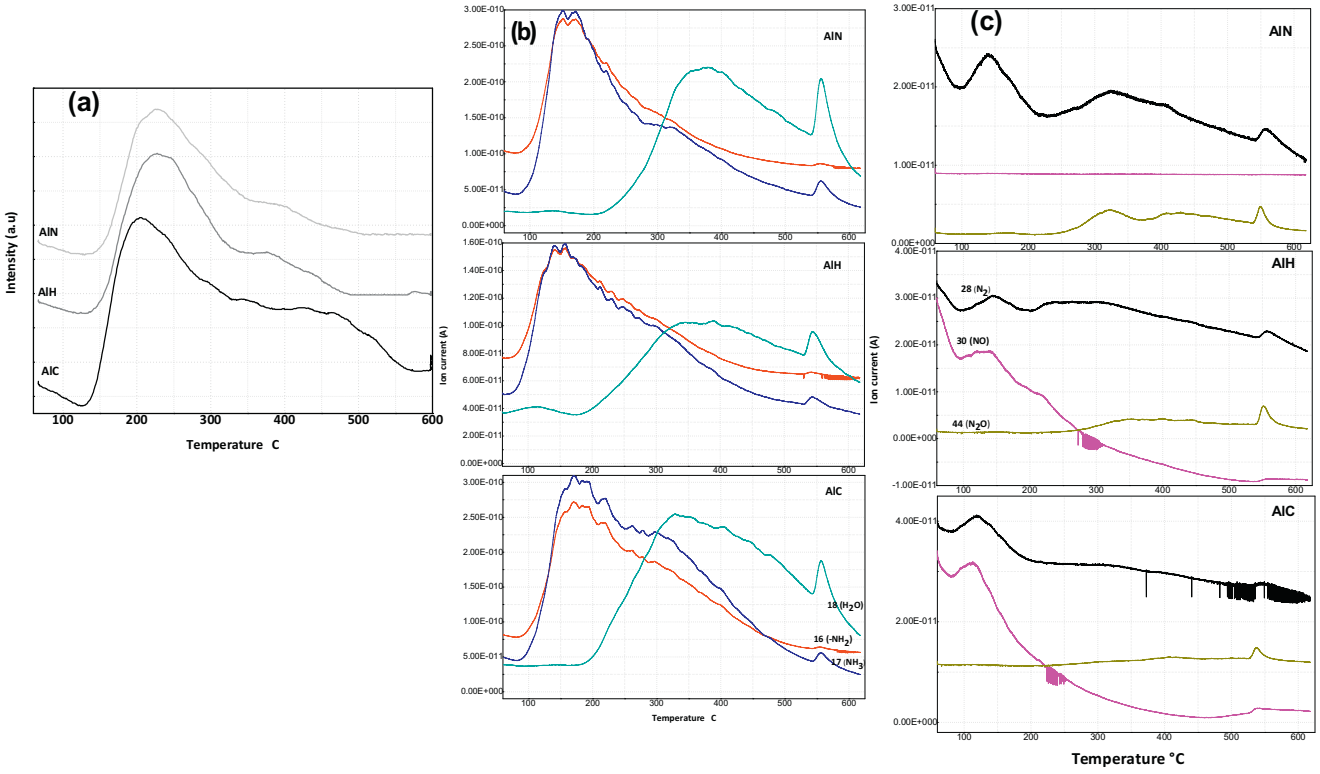

Fig. 5. (a) NH_3 TPD profiles for AlN, AlH and AlC samples (b) mass signal for $m/z = 16$ (-NH_2, red line), 17(NH_3, blue line) and 18 (H_2O, green line) (c) mass signal for $m/z = 28$ (N_2 black line), 30 (NO, pink line) and 44 (N_2O gray line). (For interpretation of the references to color in this figure legend, the reader is referred to the web version of this article.)

the BE of WO_2 in $Sb(W,V)O_4$ rutile phase reported at 246.5 eV [8]. In this study, the BE of $W4d_{5/2}$ recorded in the range of 247–247.4 eV which is intermediate between WO_3 and WO_2 BE. The results suggest the presence of W^{+6} and W^{+4} species in all the three catalysts.

Among the fresh catalysts AlC showed higher alumina content near the surface (Table 2) which indicates the greater dispersion of V, Sb and W oxides [8] on its surface. The result are in good agreement with XRD and pore volume data. According to the authors [25], the redox process between V^{+5} and Sb^{+3} generates the reduced V^{+4}/V^{+3} species and oxidized Sb^{+4}/Sb^{+5} species under the catalyst calcination conditions. In the present study, the surface existence of $V^{+4/+5}$, $Sb^{+4/+5}$ and $W^{+4/+6}$ species in different concentrations (Table 2) suggest the presence of active V–Sb–W phase to a different extent on the surface of Al_2O_3 synthesized from aluminum nitrate, aluminum hydroxide and aluminum chloride precursors.

3.6. NH_3 TPD mass (MS) study

In general, acrylonitrile selectivity depends on ammonia sorption ability of the surface active sites on the employed catalyst for the propane ammoxidation reaction. In the present study, thermally induced NH_3 sorption results on AlN, AlH and AlC catalysts are present in Fig. 5a. These measurements provide an important information about the nature of surface active sites on $V–Sb–P–W/Al_2O_3$ catalyst. Fig. 5a shows two distinct desorption peaks for all the three catalysts. The first peak pronounced in the temperature range of 150–350 °C with peak maxima around 225 °C. The later broad desorption appeared in the temperature range of 340–500 °C for AlN and AlH samples. On the other hand, for AlC the later desorption was extended in the temperature range of 300–580 °C. The earlier desorption was due to the acid sites of weak strength and the later desorption was associated with acid sites of moderate/strong strength on $V–Sb–P–W/Al_2O_3$ catalyst. Among the studied catalysts, the maximum ammonia desorption was observed on AlC (185 $\mu mol\ g_{cat}^{-1}$) over AlH (178 $\mu mol\ g_{cat}^{-1}$) and AlN (160 $\mu mol\ g_{cat}^{-1}$) samples. The acid strength of Al_2O_3 was strongly enhanced by the incorporation of Cl^{-} into or on the surface during the impregnation with solutions containing chloride precursors of an active component or by deposition of $AlCl_3$ [26]. Therefore, we strongly believe that the enhancement of the acid strength on AlC was associated with residual Cl^{-} on its surface and/or in the bulk of catalyst as established by XPS and EDS.

The corresponding TPD mass signals with $m/z = 16$ (–NH_2), 17 (NH_3), 18 (H_2O), 28 (N_2), 30 (NO) and 44 (N_2O) was recorded for

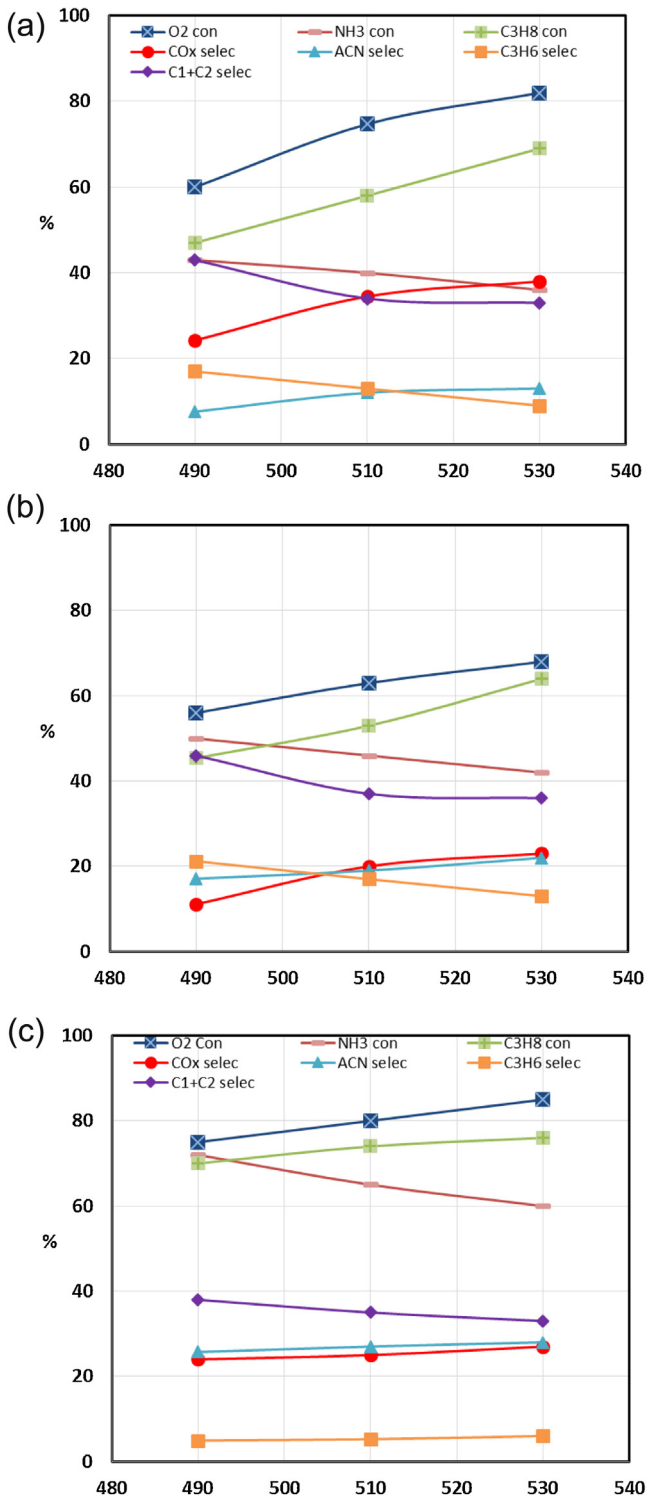

Fig. 6. Catalytic activity results on (a) AlN (b) AlH and (c) AlC samples. (For interpretation of the references to color in this figure legend, the reader is referred to the web version of this article.)
Reaction conditions: catalyst weight 4.6 g, particle size 0.5–2.0 mm, W/F = 2.8 g_{cat} s ml^{-1}, feed composition: 19.11% oxygen, 12.74% ammonia and 6.37% propane balanced helium.

AlN, AlH and AlC catalysts. Fig. 5b shows two mass signals for NH_3 (blue line) in the temperature range of 50–450 °C and 540–600 °C for all the three samples. The first mass signal showed peak maxima at 180 °C with a shoulder at 325 °C. And the second signal showed peak maxima at 565 °C. The mass signal at 180 °C ascribed to physisorbed NH_3 and the signal appeared at 325/565 °C attributed to chemisorbed NH_3 on the surface of the V–Sb–P–W/50% Al_2O_3 catalyst. The mass signal observed for $-NH_2$ (Fig. 5b, redline) species was identical to NH_3 mass signal in terms of temperature range and maxima. The results indicate that the similar nature of catalyst surface sites performing unchanged ammonia desorption and ammonia oxidation to some extent to form $-NH_2$ species. One of the ammonia degraded product water (H_2O) showed three mass signals in the temperature range of 80–180 °C (peak maxima at 130 °C), 190–540 °C (peak maxima at 360 °C) and 540–600 °C (peak maxima at 565 °C) for all the three samples (Fig. 5b, green line). The formation of water at 130 °C was due to adsorbed NH_3 reacts with very active and weekly existing O^- and O^{2-} species on the catalyst surface. Whereas, the water formed at 360 and 565 °C might be associated with adsorbed NH_3 reacts with lattice oxygen diffusing from the bulk up to the surface of the catalyst.

Further, oxidation of adsorbed $-NH_2$ species produces degraded products like N_2 and NO_x. The N_2, NO and N_2O product distribution on AlN, AlH and AlC catalysts are present in Fig. 5c. For AlN, the N_2 and N_2O mass signal observed at signal maxima 140, 325, 410 and 550 °C. It is noteworthy, that nitric oxide (NO) formation was not detected on this catalyst and the reason for it is unknown at this moment. On the other hand, N_2, NO and N_2O mass signal observed at signal maxima 140, 225, 325 and 550 °C on AlH catalyst. However, on AlC only two mass signal maxima recorded for N_2, NO and N_2O at 125 and 550 °C. In addition, a steady mass signal proceeds without registering any peak maxima in the temperature range of 225–500 °C for N_2 and N_2O on AlC catalyst. The results indicate that the moderate/strong acid sites have very wide distribution on AlC to decompose the adsorbed $-NH_2$ species. Whereas, the moderate/strong site distribution (200–500 °C) was more prominent on AlN and AlH and hence desorbed considerable amount of $-NH_2$ decomposed species such as N_2 and N_2O. Thus, the residual chlorine tuned the moderate/strong acid site density and distribution on AlC which intern influence the acrylonitrile selectivity. It was reported that the lattice oxygen participates in the formation of the surface intermediate $-NH_2$ and both lattice and weekly adsorbed oxygen species (O_2^- and O^-) are active for the conversion of the intermediate ($-NH_2$) into N_2 and NO_x [27]. It is notable that the O 1s XPS surface composition for AlN and AlH showed high amount of lattice and isolated oxygen species (O_2^- and O^-) compared to AlC.

3.7. Catalytic activity

Fig. 6a–c shows the ammoxidation reactant (propane, O_2 and NH_3) conversion and (ACN, C_3H_6, CO_x and C1+C2) product selectivity results on AlN, AlH and AlC catalysts in the temperature range of 490–530 °C at W/F = 2.8 g_{cat} s ml^{-1}. Bulk $AlPO_4$ employed as a catalyst for the ammoxidation of 2-methyl pyrazine to 2-cyanopyrazine and its minor catalytic activity was attributed to its acid sites of weak strength [28]. In the present work, $AlPO_4$ contribution for propane ammoxidation can not be ruled out. The bulk of $V_{1.0}$–$Sb_{3.5}$–$P_{0.5}$–$W_{1.0}$ catalyst showed O_2, propane and NH_3 conversion of 90, 40 and 95% respectively, with 20% slelctivity to propylene and 8% selectivity to ACN at 530 °C. Among the supported catalysts, the maximum conversion of O_2 (85%), propane (76%) and NH_3 (60%) was observed on AlC at 530 °C. Propane and O_2 conversion was increased with increase in the reaction temperature for all the three catalysts. The increasing order of O_2 and propane conversion for the studied catalysts as follows: AlH < AlN < AlC. On the other hand, NH_3 conversion decreased with increase in the reaction temperature as shown in Fig 6a–c. This was associated with high degree of reduction of the catalyst due to high CO_x formation and as a consequence poor surface oxygen availability lead to insufficient ammonia oxidation. According to Nilsson et al. [8] NH_3 conversion

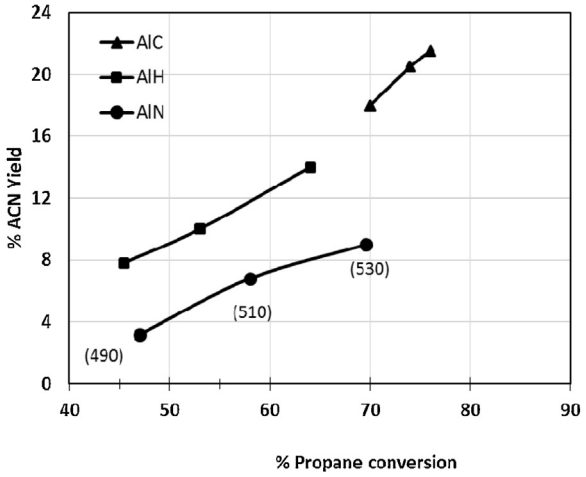

Fig. 7. Propane conversion versus ACN yield on AlN, AlH and AlC samples. Reaction conditions: temperature 490–530 °C mentioned in brackets in graph, catalyst weight 4.6 g, W/F = 2.8 g_{cat} s ml^{-1}, feed composition: 19.11% oxygen, 12.74% ammonia and 6.37% propane balanced helium.

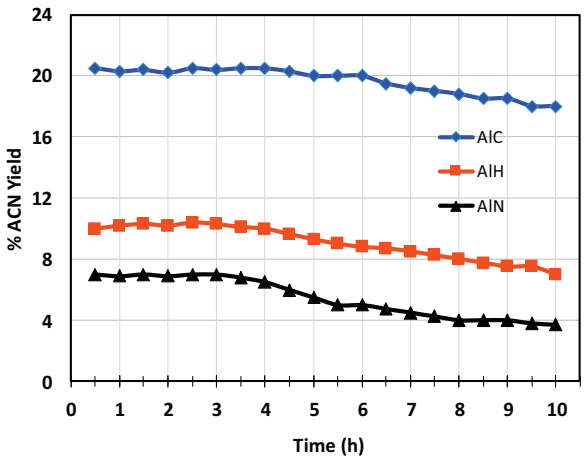

Fig. 8. Stability studies on AlN, AlH and AlC samples. Reaction conditions: temperature 510 °C, catalyst weight 4.6 g, W/F = 2.8 g_{cat} s ml^{-1}, feed composition: 19.11% oxygen, 12.74% ammonia and 6.37% propane balanced helium.

decreased with increase in C3-product (C_3H_6 and ACN) selectivity. Essentially, the greater propane conversion on AlC was associated with active surafce enriched in V–Sb–W phase. However, the slight increase in the propane and O_2 conversion on AlN over AlH might be associated with prominent Sb–W–O related phase as established by HAADF/EDS.

Among the catalysts, AlH showed maximum selectivity to propylene (21%) followed by AlN (17%) and AlC (5%) at 490 °C (Fig. 6a–c, gold colour line). The other proapne/propylene degarded products such as CH_4 and C_2H_4 formation was found to be high on AlN and AlH compared to AlC (Fig. 6, purple line). The maximum CO_x selectivity of 38% was obtained on AlN followed by AlC (26%) and AlH (23%) at 530 °C (Fig. 6a–c, red line). The slight decrease in the CO_x selectivity on AlH compared to AlC was associated with its low propane and O_2 conversions. It is clear from the result that AlN and AlH surface with V–Sb–W + Sb–W–O related phase was capable of doing propane dehydrogenation as well as propane/propylene degradation. Nilsson et al. [8] have also reported greater slectivity to C1 + C2 products on Sb-W/Al catalyst due to propane/propylene degradation.

The maximum ACN selectivity of 28% was observed on AlC over AlH (22%) and AlN (13%) at 530 °C in Fig. 6a–c (pale blue line). According to Ref. [8] the acrylonitrile yield/selectivity increased with increase in propane conversion on V–Sb–W/Al_2O_3 catalyst. To some extent, the lower propylene yield on AlC was endorsed to its higher selectivity to acrylonitrile. The lower slectivity for acrylo nitrile on AlN and AlH was attributed to degartion of adsorbed NH_3 to N_2/NO_x to a greater extent as established by the NH_3 TPD mass results (Fig. 5c). On the otherhand, higher adsorption ability for NH_3 in the presence of residual chloride followed by facile nitrogen insersion on AlC led to higher ACN selectivity. The presence of chloride plays an important role for the reforming process on Pt–Al_2O_3 catalysts [29]. The catalytic activity data in Fig. 6a–c clearly demonstrates the better catalytic properties of AlC compared to AlH and AlN catalysts.

Fig. 7 illustrates propane conversion versus ACN yield on AlN, AlH and AlC catalysts in the temperature range of 490–530 °C at W/F = 2.8 g_{cat} s ml^{-1}. The maximum ACN yield of 21.5% was observed on AlC at 530 °C. Whereas, AlH and AlN showed 14 and 9% of ACN yield respectively, at 530 °C. The greater ACN yield on AlC was associated with (i) active surface enriched in V–Sb–W phase (ii) high adsorption ability for NH_3 followed by facile nitrogen insersion tendency on chlorinated Al_2O_3 precipitated from $AlCl_3$.

3.8. Catalyst stability study

The stability of the AlN, AlH and AlC catalysts are studied for 10 h at 510 °C with W/F = 2.8 g_{cat} s ml^{-1} and the results are presented in Fig. 8. Among the catalysts, AlC showed steady ACN yield for 6 h, whereas, AlH and AlN showed 4 h of consistentcy towards ACN production under the studied propane ammoxidation conditions. The gradual decrease in the ACN yield might be associated with loss of chloride during the catalytic process for AlC and or deactivation due to the water generated in the reaction. The other possibility for decrease in the ACN yiled might be associated with agrregrated or large V–Sb–W crystallite on AlN and AlH as evidenced by fresh/spent catalyst X-ray patterns. The catalytic results in the present study appear rather unproductive in terms of acrylonitrile yield, however, they can be of interest if a process integrated with recycling of the reaction feeds which usually take place in an industrial application. Further, the AlC catalytic aspects can be improved by feeding CCl_4 as a precursor of the surface chloride promoter for this reaction. The present catalytic results are compared with other catalytic systems such as Ca–Bi–Mo [30], Mo–V–Nb [31], V/$AlGaPO_4$ [32] and Fe–Bi/SiO_2 [3] studied for propane ammoxidation. About 15% propane conversion with 28% ACN selectivity was obtained on Ca–Bi–Mo catalyst at 500 °C. High amounts of acetonitrile (19%) with small portion of ACN (9%) and propylene (4%) formation was observed on Mo–V–Nb–O catalyst at 500 °C. At 5 wt.% V loading the galium phosphate catalyst only showed 20% propane conversion with 10% ACN selectivity at 500 °C. The Fe–Bi catalyst showed only 10% yield of ACN with 20% propane conversion at 500 °C. In the present study, V–Sb–P–W/Al_2O_3 catalyst showed 20.5% ACN yield at 510 °C and it can be improved by changing the feed composition and contact time.

The plausible propane ammoxidation to acrylonitrile, CO_x and NO_x pathways based on Figs. 6 and 7 and NH_3TPD mass results are discussed here. The decrease in the propylene selectivity followed by improved ACN selectivity (or yield) with respect to reaction temperature suggests the ACN formation through propylene route for all the three catalysts. The detection of acrolein/acrylic acid in the reaction stream (Section 2.6) further strenthens the propylene oxidation to acrolein/acrylic acid route. In addition, NH_3 sorption and $-NH_2$ species formation (mass analysis, Fig 5b) on V–Sb–P–W/Al_2O_3 catalysts in the reaction temperature zone indicates the possible nitrogen insersion in acrolein/acrylic acid to produce ACN. Hence, the sucessive route for conversion of propane to ACN associated with: propane to propylene to acrolein/acrylic

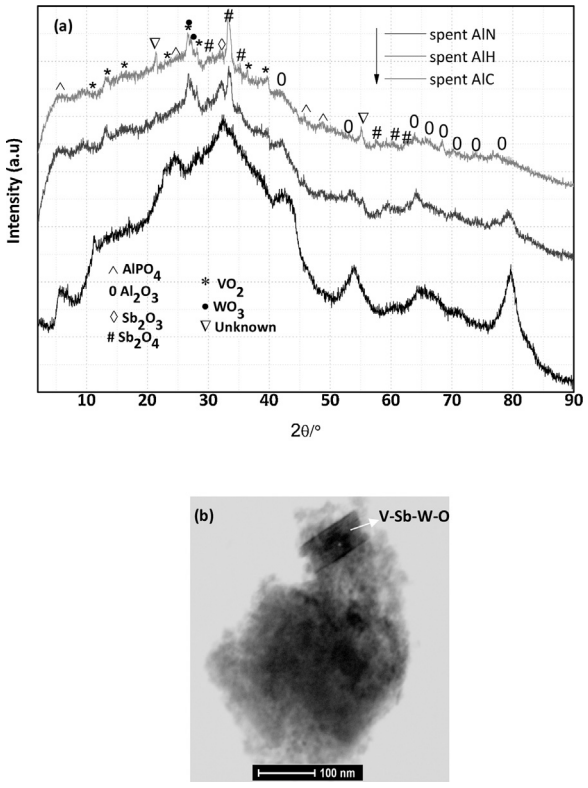

Fig. 9. (a) Spent catalyst XRD (b) spent AlC HAADF image.

acid to ACN on V–Sb–P–W/Al_2O_3 catalysts. The decrease in the C1 + C2 product selectivity followed by improved CO_x slectiivty with respect to reaction temperature suggests CO_x formation through the decomposition of C1 + C2 products to some extent in parallel on V–Sb–P–W/Al catalysts. The CO_x and hydrocarbon (C1 + C2 products) formation through propane/proylene degradation was also observed on V–Sb–W/Al_2O_3 catalyst [27,8]. Based on NH_3 TPD mass results, the formation of N_2, NO_x and H_2O indicates the parallel decomposition of ammonia on V–Sb–P–W/Al_2O_3 surface under propane ammoxidation conditions.

Fig. 9a shows the X-ray pattern of spent AlN, AlH and AlC smples. Identical X-ray pattern pronounced in spent and fresh AlN and AlH catalysts due to γ-Al_2O_3, $AlPO_4$, VO_2, WO_3, antimony oxide and an unknown phases. The results indicate that during the propane ammoxidation the surface changes were limited on AlN and AlH. This might be associated with large size crystals of V–Sb–W and Sb–W–O related phase. On the other hand, the spent AlC (Fig. 9a) retains $AlPO_4$ and γ-Al_2O_3 phases after the propane ammoxidation. However, Sb_2O_4, VO_2 and WO_3 related pattern were minimized, instead a broad pattern was observed in the 2θ range of 26–40°. The broad X-ray pattern indicates the small size/dispersed particles of Sb_2O_4, VO_2 and WO_3. Nilsson et al. [8] reported the rutile phase ($Sb_{0.9}V_{0.9-x}W_xO_4$) enhancement in $V_{1.0}$–$Sb_{5.0}$–$W_{1.0}$/Al_2O_3 catalyst after the propane ammoxidation. The result suggest the rearrangement of oxide phase near the surface during the propane ammoxidation on AlC. To know more about the surface changes on spent AlC, the sample was further analyzed by HAADF/EDS and XPS techniques. Fig. 9b clearly shows the scattered patches of V–Sb–W particles and the results are in agreement with spent XRD data. The spent AlC XPS surface composition is listed in Table 2. The results indicate the surface enrichment of vanadium and antimony species on spent AlC over its fresh counterpart. This might be associated with diffusion of oxide from bulk to surface during the propane ammoxidation process and generated more active surface compared to AlN and AlH catalysts.

4. Conclusions

- Nebulous and warm like morphology was observed for Al_2O_3 synthesized from aluminum hydroxide and aluminum nitrate precursors. On the other hand, only nebulous Al_2O_3 observed for aluminum chloride precursor.
- Enrichment in V–Sb–W phase was observed on nebulous Al_2O_3. Whereas, Sb–W–O related phase was observed on warm like Al_2O_3.
- High sorption ability for ammonia on Al_2O_3 synthesized from $AlCl_3$ was likely due to the presence of residual chloride on its surface and/or in the bulk of the catalyst.
- Among the precursors studied, Al_2O_3 synthesized from $AlCl_3$ showed maximum catalytic activity in terms of propane conversion (76%) and ACN yield (21.5%) at 530 °C.
- AlH and AlN generates the surface with large size V–Sb–W and Sb–W–O related phase which intern performs the propane dehydrogenation to propylene followed by its degradation to CO_x. The low adsorption ability for ammonia and prominent formation of NO_x on AlH and AlN further indicates the nitrogen insersion step was slow in the intermediate molecule of propane to yield ACN.

Acknowledgements

SABIC Chair of Catalysis, King Abudulaziz University is greatly acknowledged for their financial support to this work. Special thanks to Mohammed Raoof Ahmed Rafiqui for supplies/hardware support.

References

[1] R.K. Grasselli, Chapter 5, Ammoxidation of propylene and propane to acrylonitrile, RSC Nanoscience & Nanotechnology, No. 19, Nanostructured Catalysts: selective oxidations P96.
[2] Acrylonitrile World Supply Demand Report, 2013.
[3] R.D. Adams, G. Elpitiya, K. Khivantsev, D. Blom, O.S. Alexeev, M.D. Amiridis, Appl. Catal. A: Gen. 501 (2015) 10–16.
[4] M.O. Guerrero-Pérez, M.A. Pena, J.L.G. Fierro, M.A. Banares, Ind. Eng. Chem. Res. 45 (2006) 4537–4543.
[5] S. Albonetti, G. Blanchard, P. Burattin, S. Masetti, A. Tagliani, F. Trifirò, Catal. Lett. 50 (1998) 17–23.
[6] M.A. Soria, P. Ruiz, E.M. Gaigneaux, Catal. Today 203 (2013) 40–47.
[7] J.F. Brazdil, A.T. Guttmann, US patent. No. 4,873,215 (1989).
[8] J. Nilsson, A.R. Landa-Canovas, S. Hansen, A. Andersson, J. Catal. 186 (1999) 442–457.
[9] J. Nilsson, A.R. Landa-Canovas, S. Hansen, A. Andersson, J. Catal. 160 (1996) 244–260.
[10] E. Mamedov, Appl. Catal A: Gen. 474 (2014) 34–39.
[11] G. Centi, S. Perathoner, F. Trifirb, Appl. Catal. A: Gen. 157 (1997) 143–172.
[12] E. Mikolajska, E.R. Garcia, R.L. Medina, A.E. Lewandowska, J.L.G. Fierro, M.A. Banares, Appl. Catal. A: Gen. 404 (2011) 93–102.
[13] J. Bilde, P. Delichere, L. Burel, S. Loridant, J.M.M. Millet, Appl. Catal. A: Gen. 468 (2013) 341–349.
[14] E. Mikolajska, S.B. Rasmussen, A.E. Lewandowska, M.A. Bañares, Phys. Chem. Chem. Phys. 21 (2012) 2128–2136.
[15] W. Guojuna, Z. Shunhai, M. Xiaochun, G. Yun, L.U. Guanzhong, Rare Met. 29 (2010) 597–603.
[16] K.S.W. Sing, D.H. Everett, R.A.W. Haul, L. Moscou, R.A. Pierotti, J. Rouquerol, T. Siemieniewska, Pure Appl. Chem. 57 (1985) 603–619.
[17] A. Ersundu, M. Celikbilek, M. Baazouzi, M. Soltani, J. Troles, J. Alloys Compd. 615 (2014) 712–718.
[18] N. Pasupulety, K. Gunda, Y. Liu, G.L. Rempel, F.T.T. Ng, Appl. Catal. A: Gen. 452 (2013) 189–202.
[19] D.L. Sun, J.R. Deng, Z.S. Chao, Chem. Cent. J. 1 (2007) 27–30.
[20] A. Andersson, J.-O. Bovin, P. Walter, J. Catal. 98 (1986) 204–220.
[21] S.T. Triantafyllou, P.C. Chistidies, C.B. Lioutas, J. Solid State Chem. 134 (1997) 344–348.
[22] D.T. Clark, G.G. Roberts, R.W. Sykes, Thin Solid Films 70 (1980) 261–265.
[23] M. Demeter, M. Neumann, W. Reichelt, Surf. Sci. 454–456 (2000) 41–44.
[24] R. Nilsson, T. Lindblad, A. Anderson, J. Catal. 148 (1994) 501–513.
[25] J. Nilsson, A.L. Cfinovas, S. Hansen, A. Andersson, Catal. Today 33 (1997) 97–108.
[26] M. Che, O. Clause, Ch. Marcilly, in: G. Ertl, H. Knozinger, J. Weitkamp (Eds.), Handbook of Heterogeneous Catalysis, vol. 1, Wiley-VCH, Weinheim, 1997, p. 191.
[27] A. Hinz, A. Andersson, Chem. Eng. Sci. 54 (1999) 4407–4421.

[28] Ch. Srilakshmi, N. Lingaiah, P. Nagaraju, P.S. Sai Prasad, K.V. Narayana, A. Martin, B. Lucke, Appl. Catal. A: Gen. 309 (2006) 247–253.
[29] J.H. Sinfeltin, G. Ertl, H. Knozinger, J. Weitkamp (Eds.), Handbook of Heterogeneous Catalysis, vol. 4, Wiley-VCH, Weinheim, 1939.
[30] J.S. Kim, S.I. Woo, Appl. Catal A: Gen. 110 (1994) 173–184.
[31] M.O. Guerrero-Pérez, J.N. Al-Saeedi, V.V. Guliants, M.A. Bañares, Appl. Catal. A: Gen. 260 (2004) 93–99.
[32] M.A. Soria, P. Ruiz, E.M. Gaigneaux, Catal. Today 203 (2013) 40–47.